Modeling the effects of electrolyte diffusion and paste conductivity on lead/acid battery performance

Philip W. Appel, Dean B. Edwards and Thomas Stalick
University of Idaho, Moscow, ID 83843 (USA)

(Received August 8, 1992; accepted in revised form May 24, 1993)

Abstract

Two physical mechanisms normally prevent the positive active material in a lead/acid battery from reacting. One of these mechanisms is the change in plate conductivity that occurs when conductive active material is converted to nonconductive lead sulfate. The other mechanism is electrolyte diffusion. This paper presents a model that combines the effect of both these mechanisms on the discharge capacity of a lead/acid battery for constant current discharge. The model characterizes the electrolyte diffusion in a cell with two equations. A finite difference equation characterizes the diffusion process between the plates, and a McLaurin series approximate the electrolyte diffusion inside the positive plate. The electrolyte stored inside the plate, before the discharge begins, also contributes to the cell's capacity and is included in the model. The critical volume fraction characterizes the conductivity of the positive active material. A sharp decrease in conductivity occurs when the amount of active material, that has reacted in a plate, reaches this fraction. A computer program combines these diffusion and conductivity models into one comprehensive model. The simulated data from this model are compared with experimental data previously reported [1].

Introduction

Several mechanisms can limit the capacity of a lead/acid battery. The diffusion of the sulfate ion into the positive plate of the battery is an important capacity-limiting mechanism as previously discussed by other authors [2–4]. This effect is most noticeable during medium to high discharge rates. At low discharge rates, electrical conductivity of the positive active material limits the reaction [5–7]. To better understand these limitations, a computer model that simultaneously includes the effect of both these mechanisms on the discharge capacity of a lead/acid battery was developed.

Several researchers [3, 4, 8–10] have previously modeled diffusion in lead/acid batteries. Stein [3] and Horvàth *et al.* [4] studied the electrolyte diffusion using Fick's laws of diffusion. Papazov [8] used mass-transport theories to model the movement of the reactants in a cell. Maja and Penazzi [9] modeled the sealed gas recombinant battery by analyzing the gas-material balance with in the cell. Ekdunge and Simonson [10] modeled the kinetics of the electrode process, the ionic mass transport and the effects of structural changes. The model presented here uses Fick's first and second laws of diffusion to model the diffusion of the acid between the plates. The concentration of the acid inside the plate is approximated by a second order MacLaurin series expansion.

0378-7753/93/$6.00

Researchers [4, 5, 7, 11–14] have also developed current distribution and conductivity models for the lead/acid battery. Simonsson [7] evaluated the current distribution of the battery during discharge. Vaaler *et al.* [12] modeled the battery grid and active mass using Kirchoff's equations. Metzendorf [5], Pohl and Schendler [11], and Horvàth *et al.* [4] modeled the battery using electrical conductivity as the limiting mechanism. Maja *et al.* [13] have modeled the grid-active material, and the electrolyte as a series of resistors, and Winsel *et al.* [14] modeled the resistance between the active material particles.

Two authors of this paper, Edwards and Appel [15], had previously modeled the conductivity of the positive and negative active material. The conductivity of the active material changes dramatically after a critical ratio of material has reacted. After this ratio is reached, the paste becomes nonconductive and the reaction stops. The critical volume ratio, as defined by Metzendorf [5], is therefore an important parameter in this paper. The two mechanisms that limit capacity, electrolyte diffusion and active-material conductivity, were combined so that both the high- and low-rate battery capacities could be predicted.

The model will generate both voltage versus discharge-time plots and capacity curves. A capacity curve shows the percent of the positive active mass that reacts as a function of the discharge rate. The computer generated voltage versus time plots and the capacity curves are compared with the experimental data previously reported [1].

The model presented in this paper can be used to predict and help understand the behavior of plates with active material additives. In a companion paper [16], this model will be used to simulate the effects that hollow borosilicate glass microspheres have on the positive active mass.

Model development

The model solves for the acid concentration between the plates with a finite difference solution of Fick's laws. In the solution, the concentration gradients at the surface of both plates are assumed to be constant. These boundary conditions are valid for constant current discharges. The solution of the finite difference equations provides the acid concentration at the plate's surface.

A MacLaurin series expansion estimates the acid concentration inside the plate where the reaction occurs. The expansion uses the acid concentration and its spatial derivatives at the plate's surface to develop an expression for the acid concentration as a function of distance into the plate. After the discharge into the plate where the reaction occurs, called the reaction distance, is determined, the acid concentration at the reaction distance can be found and the cell voltage calculated.

The reaction discharge depends on a number of factors. These factors include the amount of active material that had previously reacted during a discharge, the critical volume fraction, and the amount of electrolyte stored in the plates. In subsequent sections these factors are combined to estimate the reaction distance. After the acid concentration at the reaction distance is established, voltage versus time and capacity curves can be calculated.

Modeling the concentration between the plates

Fick's first law of diffusion can be written:

$$J = -D\frac{\partial m}{\partial x} \tag{1}$$

where J is the flux of the ions past a plane, D the steady-state diffusion rate, m the ion concentration and x the distance in the ion movement direction. This equation makes the assumptions that the ions diffuse only in a linear direction and that the diffusion rate is constant and independent of ion concentration. The steady-state diffusion rate at 25 °C was reported by Bode [2] as 3.56×10^{-9} m^2/s (2.081×10^{-9} in^2/s).

The spatial and transient distribution of the acid concentration follows Fick's second law of diffusion:

$$\frac{\partial m}{\partial t} = D\frac{\partial^2 m}{\partial x^2} \tag{2}$$

Both forms of Fick's laws assume that the ion migration is strictly due to a concentration gradient. The ion concentration between the plates is determined for both position and time by using a finite difference solution to Fick's second law of diffusion. The Crank–Nicholson [17] method provides an implicit finite difference technique which is second order accurate with both time and space.

The Crank–Nicholson method forms a tridiagonal matrix using the approximation:

$$\frac{\partial^2 m}{\partial x^2} \simeq \frac{1}{2}\left(\frac{m_{k+1}^{j}-2m_k^{j}+m_{k-1}^{j}}{(\Delta x)^2} + \frac{m_{k+1}^{j+1}-2m_k^{j+1}+m_{k-1}^{j+1}}{(\Delta x)^2}\right) \tag{3}$$

where j represents the time counter and k the x position counter. This equation along with the approximation:

$$\frac{\partial m}{\partial t} \simeq \frac{m_k^{j+1}-m_k^{j}}{\Delta t} \tag{4}$$

can be used to create a Jacobian matrix solution to eqn. (2). The general equations in the Jacobian will have the form:

$$-\lambda m_{k-1}^{j+1}+2(1+\lambda)m_k^{j+1}-\lambda m_{k+1}^{j+1} = \lambda m_{k-1}^{j}+2(1-\lambda)m_k^{j}+\lambda m_{k+1}^{j} \tag{5}$$

where $\lambda = D\ \Delta m/\Delta x^2$.

For a constant current discharge, the concentration gradient at the boundary is constant and known. For the left boundary node, which is the negative plate, eqn. (5) can be written as:

$$2(1+\lambda)m_1^{j+1}-\lambda m_2^{j+1} = \lambda f_0(t^j)+2(1-\lambda)m_1^{j}+\lambda m_2^{j}+\lambda f_0(t^{j+1}) \tag{6}$$

and for the right boundary node, which is the positive plate, as:

$$-\lambda m_{B-1}^{j+1}+2(1+\lambda)m_B^{j+1} = \lambda f_{B+1}(t^j)+2(1-\lambda)m_B^{j}+\lambda m_{B+1}^{j}+\lambda f_{B+1}(t^{j+1}) \tag{7}$$

The subscript B represents the node at the right boundary.

The concentration gradients at the negative and positive plates are the boundary conditions for eqns. (6) and (7), respectively. Stein [3] used Fick's first law (eqn. (1)) to develop an expression for these boundary conditions as:

$$\frac{dm}{dx} \simeq \frac{i}{D}\frac{\partial H}{\partial q} \tag{8}$$

where i represents the current density, and $\partial H/\partial q$ is the change in acid concentration per Coulomb of charge transport. The values reported by Stein [3] for $\partial H/\partial q$ at the positive plate is -7.15×10^{-6} mol/C and 1.97×10^{-6} mol/C for the negative plate.

The system was modeled as forty nodes between the positive and negative plates. Where the plates were modeled as 0.1 inches apart (approximately the thickness of the separator) and a time step of one second was used. A one second time step was chosen to ensure a stable solution. The resulting 40 by 40 Jacobian matrix is then:

$$[C][m]=[K] \tag{9}$$

where m is the concentration solution, C the Jacobian matrix, and K the concentration matrix from the previous time step.

Solutions of eqn. (9) are plotted as a function of the position between the plates. An example of a set of data from a representative discharge is given in Fig. 1. The dotted lines at the left and right side of this Fig. are the positions of the negative and the positive plate, respectively. Note that the right side of the Fig. has a steeper slope, caused by water being produced at the positive plate. The water generation dilutes the acid at the boundary creating the slope change. Figure 1 represents a medium discharge rate (i.e. 0.06 A/g of positive active material), and shows only one solution for every 500 time steps.

The solution discussed so far only represents the concentration between the plates. Equation (9) assumes that the reaction occurs on the surface of the plates. It does not account for the diffusion of the acid into the plate where the reaction actually occurs. Concentrations inside the plate will be lower than on the surface and this difference must be included in the analysis. Figure 1 shows a projection of the concentration into the positive plate. This projection is shown as a series of lines located to the right of the second dotted line. A MacLaurin series expansion is used to approximate the concentration where the reaction occurs and will be discussed in the next section.

Modeling the concentration within the plate

The concentration within the positive plate for constant current discharges is approximated by a MacLaurin series expansion. This expansion provides the molar concentration, m, at some distance, x_p, from the plate's edge, and is given by the following equation:

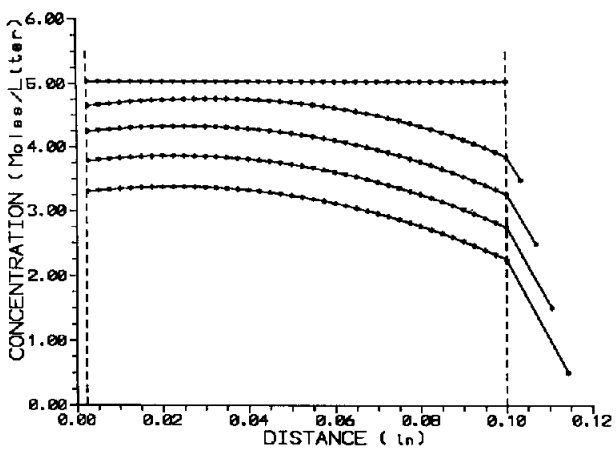

Fig. 1. Concentration vs. distance at different times of a discharge (0.06 A/g discharge).

$$m(x_p)=m\Big|_{x_p=0+}+x_p\frac{\partial m}{\partial x_p}\Big|_{x_p=0+}+\frac{x_p^2}{2!}\frac{\partial^2 m}{\partial x_p^2}\Big|_{x_p=0+}+\ldots \tag{10}$$

The distance x_p has been nondimensionalized relative to half the plate thickness. Therefore, the value of x_p will be one at the center of the plate and zero at the surface of the plate. The first and second spatial derivatives of the concentration curve are used in this approximation while the higher order terms are neglected. It should be noted that the concentration and derivatives used in eqn. (10) are evaluated to the right of the discontinuity that exists at the positive plate's boundary. However, these terms can be derived from the boundary conditions that exist to the left of this discontinuity.

The first term, which is the concentration at $x_p=0^+$, must be the same on both the left and right side of the boundary. If this condition were not true, a step change in concentration would exist and cause an infinite flow of ions, thereby eliminating any difference in concentration. The concentration m_B at the positive plate's surface, which was previously determined using the finite difference equation (eqn. (9)), will therefore be equal to the concentration $m|_{x_p=0+}$ on the other side of the discontinuity.

In eqn. (1), the flux of ions, J, moving across the boundary must be the same from mass conservation. This results in the condition that:

$$J=-D\frac{\partial m}{\partial x}\Big|_{x_p=0-}=-D_p\frac{\partial m}{\partial x}\Big|_{x_p=0+} \tag{11}$$

The first derivatives of the concentration on either side of the boundary are therefore proportional. The proportionality constant is the ratio of diffusion constants, where D is the diffusion rate in the electrolyte and D_p is the average diffusion rate in the plate.

Bode [2] reports that the average diffusion rate within the plates can be approximated by:

$$D_p\approx D\frac{\rho}{\tau} \tag{12}$$

where ρ is the porosity and τ the tortuosity. For our evaluation, the tortuosity of the plate was set equal to one. The first derivative in eqn. (10) is then equal to the first derivative evaluated to the left of the boundary multiplied by the ratio of the diffusion constants, D/D_p. Since for a constant current discharge, the first derivative located to the left of the discontinuity is constant and known, the second term in eqn. (10) is:

$$\frac{\partial m}{\partial x}\Big|_{x_p=0+}=\frac{D}{D_p}\frac{\partial x}{\partial x}\Big|_{x_p=0-} \tag{13}$$

The second spacial derivatives on both sides of the boundary can also be related. The change in concentration with respect to time must be the same on both sides of the boundary or else, after a finite time, a step change in concentration would exist across the boundary. Using eqn (2), the second spatial derivatives across the boundary are:

$$\frac{\partial m}{\partial t}=D\frac{\partial^2 m}{\partial x_p^2}\Big|_{x_p=0-}=D_p\frac{\partial^2 m}{\partial x_p^2}\Big|_{x_p=0+} \tag{14a}$$

or,

$$\left.\frac{\partial^2 m}{\partial x_p^2}\right|_{x_p=0+} = \frac{D}{D_p}\left.\frac{\partial^2 m}{\partial x_p^2}\right|_{x_p=0-} \tag{14b}$$

Although the second spatial derivative to the left of the boundary can be calculated each time step, for this simplified analysis only a rough estimate is used. We approximate the second spatial derivative to the left of the boundary by the following equation:

$$\left.\frac{\partial^2 m}{\partial x_p^2}\right|_{x_p=0-} \approx \frac{\left.\frac{\partial m}{\partial x}\right|_{x_p=0-} - \left.\frac{\partial m}{\partial x}\right|_{\text{center of cell}}}{x_d} \tag{15}$$

where x_d is half the linear distance between the positive and negative plates. Figure 1 shows that the first derivative is approximately zero at the center of the cell. The first derivative at the boundary is constant and known, as previously discussed. Therefore, the second derivative to the left of the boundary is approximated as the first derivative divided by one half the distance between the plates:

$$\left.\frac{\partial^2 m}{\partial x^2}\right|_{x_p=0-} = \frac{1}{x_d}\left.\frac{\partial m}{\partial x}\right|_{x_p=0-} \tag{16a}$$

and,

$$\left.\frac{\partial^2 m}{\partial x_p^2}\right|_{x_p=0+} = \frac{D}{D_p}\left.\frac{\partial^2 m}{\partial x_p^2}\right|_{x_p=0-} = \frac{D}{D_p}\frac{1}{x_d}\left.\frac{\partial m}{\partial x_p}\right|_{x_p=0-} \tag{16b}$$

As a check on the accuracy of the above estimate, the value of the second derivative estimated in eqn. (16) and the numerically evaluated second derivative were plotted against time during a representative discharge, see Fig. 2. The derivative of concentration with respect to time is calculated at each time step. As seen in Fig. 2, the second

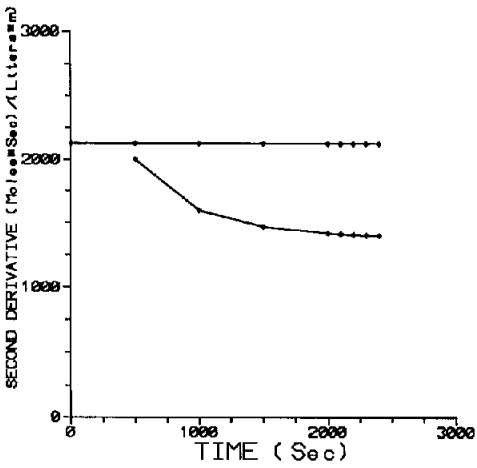

Fig. 2. The second spatial derivative of the concentration as a function of time.

derivative estimated from eqn. (15) provides a rough estimate to the numerically calculated second derivative.

After the above values are substituted into eqn. (10), the estimate for electrolyte as a function of the nondimensional distance, x_p, is:

$$m(x_p) = m_B + x_p \frac{J}{D_p}\left(\frac{\partial H}{\partial q}\right)\Big|_B + \frac{x_p^2}{2!}\frac{J}{D_p d}\left(\frac{\partial H}{\partial q}\right)\Big|_B + \ldots \tag{17}$$

where all quantities have been previously defined.

Estimating the reaction distance

Equation (10) provides an estimate for the concentration within the plate as a function of the variable x_p. The distance into the plate where the reaction is occurring will be called the reaction distance x_R. This distance depends on the critical volume fraction, V_c, which is the amount of material that can react before conductivity is lost [5]. In previous work [15], a computer model estimated the critical volume fraction to be about 60% for positive lead/acid battery plates having no additives.

The reaction distance, x_R, is determined from the discharged Ah and the critical volume fraction as shown below:

$$x_R = \frac{It}{V_c C_s} \tag{18}$$

where t is the total elapsed time, I the discharge current and C_s the stoichiometric capacity of the cell. Equation (18) assumes that the reaction starts on the edge of the plate and reacts all of the material that can be reacted (i.e., 60% of the material available for reaction) until the cell voltage drops to 1.75 V. The maximum capacity that a cell can produce is equal to V_c times the stoichiometric capacity, C_s, of the positive active material in the cell. This maximum occurs when the reaction distance reaches the center of the plate, or x_R has a value of one.

Modeling electrolyte stored in the plate

The electrolyte ions stored in the plates do not need to diffuse to react with the active material. These stored ions allow the reaction to proceed independent of the ions that diffuse into the plate. To account for these stored ions, an adjustment will be added to the elapsed time for each time step. The elapsed time adjustment, Δt, is given by the following equation:

$$\Delta t = \frac{\Delta m V_p e F}{I} \tag{19}$$

where Δm is the change in concentration where the reaction occurs from one time step to the next. The pore volume, V_p, is given for a specific type of plate, F is Faraday's constant and e the number of electrons that participate in the reaction.

Figure 3 shows the percent of positive active material as a function of distance into the plate. Two regions are shown in this Fig. The top region shows the material that reacts with the acid diffusing into the plate from the electrolyte stored between the plates. This diffusion is governed by eqn. (17) described in the previous section. The bottom region, containing the horizontal lines, shows the material that reacts with the acid stored in the pores of the plate. Each line represents a time step and the amount of material that reacts is determined by multiplying the discharge current by the time correction, eqn. (19).

The dotted line in Fig. 3 shows what a fully-discharged plate would look like. This shape is similar to the lead sulfate distribution patterns found by X-ray diffraction

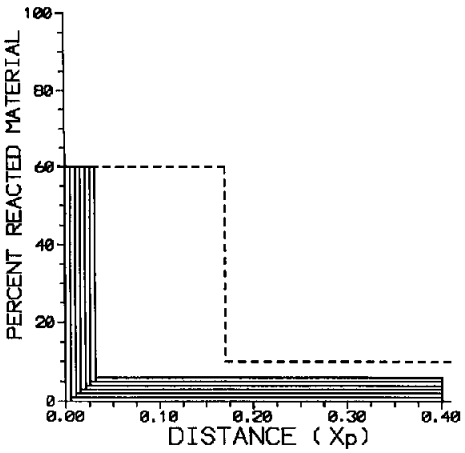

Fig. 3. Percent of reacted lead dioxide as a function of location in the plate.

work on discharged plates [2]. The electrolyte is unable to diffuse fast enough to keep up with the rate of depletion in the center of the plate. The material on the outside of the plate will therefore have a greater percent of lead sulfate than the material in the center of the plate.

Voltage versus time curves

The actual concentration gradient of the acid in a real battery is difficult to measure but battery voltage can be easily found during a discharge. The Nernst equation is used to convert the molar concentration of the acid to the electrochemical potential as shown below:

$$V = V_0 + \frac{RT}{nF} \ln([H^+]^3[HSO_4^-]) - V_{drop} \tag{20}$$

where V_0 is the standard electrochemical potential relative to a hydrogen electrode, R the universal gas constant, T the temperature, n is the number of electron participating in the reaction and F the Faraday constant. (The V_{drop} term will be discussed in the next paragraph.)

The internal resistance of the battery and other resistance terms associated with the charging station are of course not accounted for in the Nernst equation. The total resistance was estimated from experimental data. To find the total resistance of a cell, the initial voltage of the cell during discharge was recorded for various discharge rates. The voltages were plotted against the current and a linear least squares best fit line was calculated. Figure 4 gives experimental data for cell voltage as a function of current. A best fit linear equation to the experimental data, eqn. (21), is also shown in the Fig.:

$$V_{drop} = -0.2609I + 2.138 \tag{21}$$

The y-intercept point of this line represents the standard electrochemical potential of the cell being tested. This potential depends on the initial concentration. The model assumes an initial concentration of 5.04 mol/l, which corresponds to 2.14 V. Therefore the y-intercept is used to correct for any difference between the tested cell and this value. Also, the slope of the line is the combined resistance of the cell and the testing

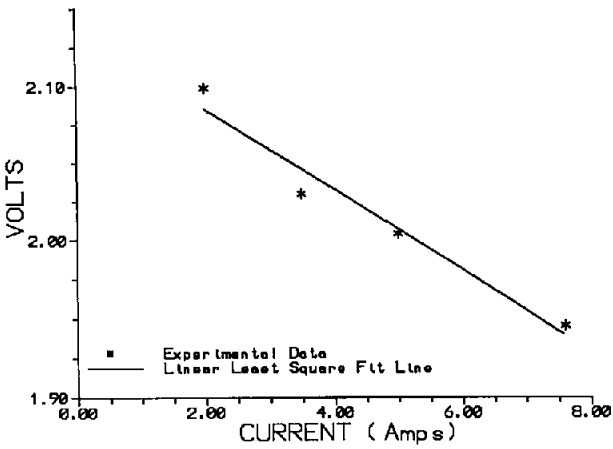

Fig. 4. Initial voltage vs. discharge rate.

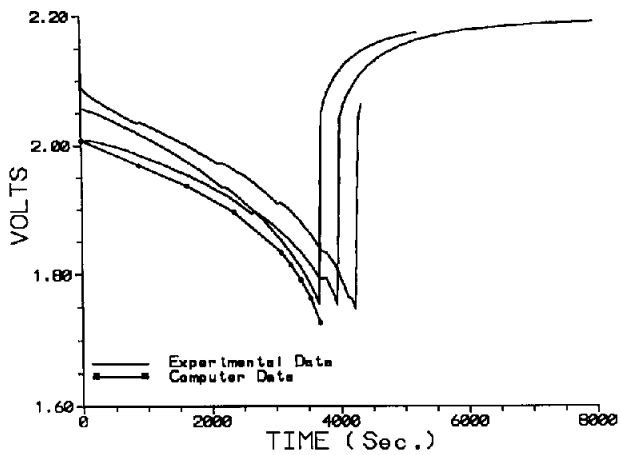

Fig. 5. Cell voltage vs. time (0.06 A/g discharge).

station. This voltage drop is then subtracted from the voltage determined by the Nernst equation.

Computer data

The model provides the voltage as a function of time for a simulated cell during constant current discharge. The time includes the time adjustment for the electrolyte stored in the plate that reacts. This computer data plus the experimental results from actual plates are shown in Fig. 5 and will be discussed in greater detail in the next section.

During the testing of the standard cells, a cutoff voltage of 1.75 V was used. Therefore, the model used this same restriction on the cell voltage. A problem arises from using a cutoff voltage of 1.75 V at high discharge rates (greater than 0.08 A g), since the resistance voltage drop limits the capacity of the battery. At these current

levels, the resistive voltage drop becomes so high that the cutoff voltage is reached before even the electrolyte stored in the plate can react.

The capacity of plates investigated in this paper are reported as a percent of their stoichiometric capacity, the theoretical number of Ah in the plate. To find the capacity of the positive plate being modeled, the total time is multiplied by the discharge current and divided by the stoichiometric capacity of the modeled plate. The total time is equal to the sum of time steps plus the time adjustments used for the stored electrolyte. The modeled capacity will be compared with experimental data in the next section.

Comparison with experimental data

Figure 5 shows a computer-generated voltage versus time curve with several experimental curves for the same constant current discharge. The experimental data come from previous work done by Edwards and Srikanth [1]. The voltage versus time plots shown in Fig. 5 are typical and illustrate some of the difficulties with the model.

The computer-generated curve's initial voltage is lower than the average initial voltage of the experimental curves. The discrepancy between the initial voltage used by the model and the experimental values can be attributed to a couple of factors. The initial concentration and resistance parameters used in the model are average values determined from experimental data for a number of different discharge rates. These parameters will therefore be in error for at least some of the discharges. The variation in the initial concentration of the experimental cells would also contribute to inaccuracies between the model's prediction and the experimental data. If the cells were discharged immediately after a charge while the electrolyte concentration in the plate was high, then the initial voltage for the experimental cells would be higher than that predicted by the model.

In Fig. 6, the voltage versus time curves generated by the model, as well as the experimental curves, for five different discharge rates are shown. To simplify the Fig., only one experimental curve is given for each computer-generated curve. Figure 6 shows that the model's voltage versus time plots match the experimental data at the beginning and the end of the discharge relatively well. However, the shape of the experimental curves differ significantly from the curves predicted by the model. This is especially true for the low discharge rates.

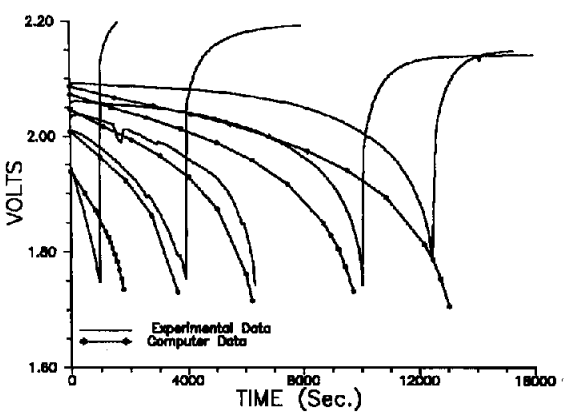

Fig. 6. Combined voltage vs. time curves for various discharge rates.

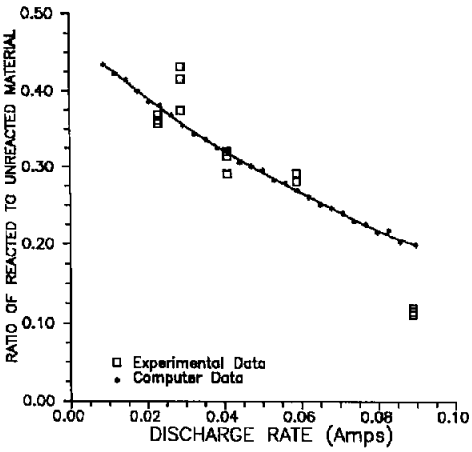

Fig. 7. Capacity vs. discharge rate.

We believe the method used to model the stored electrolyte in the positive plate is responsible for the discrepancy between the predicted and measured voltage. The model assumes that all of the acid contained in the plate's pores react to the same concentration as occurs at the reaction distance, x_R. In an actual plate, the stored electrolyte would have some concentration gradient and more of it would react earlier in the discharge than the model presently predicts. The model would therefore predict a lower voltage during the discharge than what the data show. Our model would need to be further developed to account for the gradient in the stored electrolyte to correct this problem.

Our treatment of the stored electrolyte also causes another problem. During the time-adjustment period, when the electrolyte in the plate is reacting, the concentration gradient between the plates does not change. This simplifying assumption will therefore cause the model to underpredict the electrolyte concentration in the positive plate. The cell voltage predicted by the model will be less than the measured voltage due to this time adjustment method of dealing with the stored electrolyte.

Although our treatment of the stored electrolyte inside the positive plate causes the model to underpredict the voltage over most of the discharge, the model's end-of-discharge voltage is relatively accurate. Of course, at the end of discharge, most of the electrolyte in the positive plate has reacted so that it no longer has much of an effect on the voltage. The electrolyte diffusing into the positive plate will determine the voltage at the end of discharge. The assumptions used to model the diffusion of electrolyte into the positive plate appear to work relatively well.

The more important use of this model will be in determining the capacity of new plate designs. As seen in Fig. 7, the numerically determined capacity of the modeled plates compares favorably with the experimental data reported by Edwards and Srikanth [1]. Further work is needed to verify the model at the more extreme discharge rates.

In a companion paper [16], this model is used to predict the behavior of plates having additives. The plates that are modeled contain various amounts of hollow, borosilicate glass microspheres. These spheres are nonconducting and lower the critical volume fraction, yet they also increase the amount of acid stored in the positive plate relative to the amount of active material.

Conclusions

The model presented in this paper combines diffusion and conductivity parameters to characterize constant current discharges for lead/acid batteries. Porosity, density of active material, resistance of the cell, initial concentration of the acid and critical volume fraction are the parameters required by this model to predict cell behavior. The model uses these parameters to estimate the acid concentration where the reaction occurs in the plate. This concentration is then used to calculate cell voltage as a function of time and to determine cell capacity. Although the model is relatively simple and provides reasonable estimates for a cell's capacity, the shape of the voltage versus time curves predicted by the model are different from the experimental data. This difference is a result of how the stored electrolyte in the positive plate is modeled.

References

1 D.B. Edwards and V. Srikanth, *Power Sources, 34* (1991) 217–232.
2 H. Bode, *Lead–Acid Batteries*, Wiley–Interscience, New York, 1977, p. 387.
3 W. Stein, *Thesis*, Rogowski-Institut für Elektrotechnik der Technischen Hochschule, Aachen, Germany, 1959.
4 P. Horvàth, P. Jedlovszky and M. Benedek, *J. Power Sources, 8* (1982) 41–54.
5 H. Metzendorf, *J. Power Sources, 7* (1982) 281–291.
6 P.W. Appel, *Master's Thesis*, University of Idaho, Moscow, ID, Aug. 1991.
7 D. Simonsson, *J. Electrochem. Soc., 120* (1973) 151–157.
8 G. Papazov, *J. Power Sources, 18* (1986) 337–347.
9 M. Maja and N. Penazzi, *J. Power Sources, 25* (1989) 99–109.
10 P. Ekdunge and D. Simonsson, *J. Appl. Electrochem., 19* (1989) 136–141.
11 J.P. Pohl and W. Schendler, *J. Power Sources, 6* (1981) 245–250.
12 L.E. Vaaler, E.W. Brooman and H.A. Fuggiti, *J. Appl. Electrochem., 12* (1982) 721–734.
13 M. Maja and P. Spinelli, *J. Power Sources, 30* (1990) 201–207.
14 A. Winsel, E. Voss and U. Hullmeine, *J. Power Sources, 30* (1990) 209–226.
15 D.B. Edwards and P.W. Appel, *J. Power Sources, 38* (1992) 281–286.
16 D.B. Edwards and P.W. Appel, *J. Power Sources, 46* (1993) 39–48.
17 S.C. Chapra and R.P. Canale, in A.T. Brown and S. Tenney (eds.), *Numerical Methods for Engineers*, McGraw-Hill, New York, 2nd edn., 1988, p. 812.